

ATMOSPHERIC LENSING AND OBLATENESS EFFECTS DURING AN EXTRASOLAR PLANETARY TRANSIT

LAM HUI^{1,2} AND SARA SEAGER²

Received 2001 March 20; accepted 2002 February 4

ABSTRACT

Future high-precision photometric measurements of transiting extrasolar planets promise to tell us much about the characteristics of these systems. We examine how atmospheric lensing and (projected) planet oblateness/ellipticity modify transit light curves. The large density gradients expected in planet atmospheres can offset the unfavorably large observer lens-to-source lens distance ratio and allow the existence of caustics. Under such conditions of strong lensing, which we quantify with an analytic expression, starlight from all points in the planet's shadow is refracted into view, producing a characteristic slowing down of the dimming at ingress (vice versa for egress). A search over several parameters, such as the limb-darkening profile, the planet radius, the transit speed, and the transit geometry, cannot produce a nonlensed transit light curve that can mimic a lensed light curve. The fractional change in the diminution of starlight is approximately the ratio of atmospheric scale height to planet radius, expected to be 1% or less. The lensing signal varies strongly with wavelength—caustics are hidden at wave bands where absorption and scattering are strong. Planet oblateness induces an asymmetry to the transit light curve about the point of minimum flux, which varies with the planet orientation with respect to the direction of motion. The fractional asymmetry is at the level of 0.5% for a projected oblateness of 10%, independent of whether or not lensing is important. For favorable ratios of planet radius to stellar radius (i.e., gas giant planets), the above effects are potentially observable with future space-based missions. Such measurements could constrain the planet shape and its atmospheric scale height, density, and refractive coefficient, providing information on its rotation, temperature, and composition. We have examined a large range of planetary system parameter space including the planetary scale height and orbital distance. For HD 209458b, the only currently known transiting extrasolar planet, caustics are absent because of the very small lens-source separation (and a large scale height caused by a high temperature from the small separation). Its oblateness is also expected to be small because of the tidal locking of its rotation to orbital motion. Finally, we provide estimates of other variations to transit light curves that could be of comparable importance—including rings, satellites, stellar oscillations, star spots, and weather.

Subject headings: gravitational lensing — planetary systems — stars: atmospheres

1. INTRODUCTION

The exciting discovery of the transit of HD 209458 (Charbonneau et al. 2000a; Henry et al. 2000; Jha et al. 2000) allowed the first direct measurement of the physical properties of an extrasolar planet, including its radius, and together with radial velocity measurements, its absolute mass and average density. Photometric follow-up of radial velocity planet candidates and future ground- and space-based surveys are expected to discover hundreds more transiting planets. Planned or proposed space-based missions, in particular MOST, MONS, COROT, the Eddington Telescope, and the Kepler Mission, are expected to be able to detect flux variations at the 10^{-5} level. Recent *Hubble Space Telescope* observations of the HD 209458b transit (Brown et al. 2001), with an accuracy of 10^{-4} , illustrate the capability of high-precision space-based photometry. With the anticipated large number of transiting planets and the high accuracy with which they can be monitored, it is important to explore small variations in the transit light curve that might be detectable and allow us to deduce further properties of the transiting planets.

In this paper we focus on how atmospheric refraction, which we also refer to as atmospheric lensing, or lensing for short, modifies the transit light curve. We treat the general case of an ellipsoidal planet, and the same calculation also allows us to examine the effects of (projected) planet oblateness/ellipticity, regardless of whether or not lensing is important. We examine under what conditions atmospheric lensing and oblateness signatures might be significant, detectable, and distinguishable from other effects.

We develop the lensing formalism in § 2 and contrast atmospheric lensing with gravitational lensing. For readers with a background in the latter, we point out several places where intuition gained from gravitational lensing fails for atmospheric lensing. In § 3 we give a complete list of all the parameters employed in our model. The condition under which atmospheric lensing produces strong lensing (i.e., existence of caustics) is taken up in § 4. An analytic expression describing this condition is given. We emphasize the connections between atmospheric lensing by extrasolar planets and atmospheric lensing by solar system bodies during their occultations of distant stars; the latter has long been observed (see, e.g., Elliot & Olkin 1996; Hubbard 1997 and references therein). The difference is that in the extrasolar case, the lens-source distance is much smaller than the lens-observer distance and the source is extended compared to the lens, while the opposite is true in the solar system case. In § 5.1 we examine how the lensing modifications to the

¹ Department of Physics, Columbia University, 538 West 120th Street, New York, NY 10027.

² Institute for Advanced Study, School of Natural Sciences, Einstein Drive, Princeton, NJ 08540; lhui@astro.columbia.edu, seager@ias.edu.

light curve vary with the model parameters. In § 5.2 we address the following question: to what extent can a lensed light curve be confused with a nonlensed light curve with different parameters? Similarly, in § 5.3 we isolate characteristic modifications by the planet's oblateness to the transit light curve. The issue of how absorption affects the color dependence of lensing is taken up in § 6, where we also discuss how lensing impacts the planet transmission spectrum. Finally, we conclude in § 7 with a summary and with a list of other effects that might be of comparable magnitude to the lensing and oblateness signatures.

An interesting paper by Hubbard et al. (2001) recently appeared as our paper was nearing completion. They discussed some of the same issues addressed here but focused mainly on detailed predictions for the case of HD 209458b. They also presented calculations of atmospheric glow from Rayleigh scattering, which we do not treat in this paper, although we do discuss extinction by Rayleigh scattering.

2. THE LENSING MODEL

2.1. Formalism

Much of the formalism presented here closely parallels that used for gravitational lensing, and the similarities and differences are discussed in § 2.2. Equivalent techniques have been applied to lensing of distant stars by solar system bodies (Elliot & Olkin 1996; see also Draine 1998 for a treatment of gaseous lensing by large spherical clouds). Ray optics provide the following starting point for lensing:

$$\theta_S = \theta_I + \theta_D \frac{D_{LS}}{D_{OL} + D_{LS}}, \quad (1)$$

where θ_D is the angle of deflection, θ_S and θ_I are the source and image positions, respectively, D_{LS} denotes the distance between the lens and the source, and D_{OL} is the separation between the lens and the observer (a schematic ray-tracing diagram is given in Fig. 1). The angle of deflection is deter-

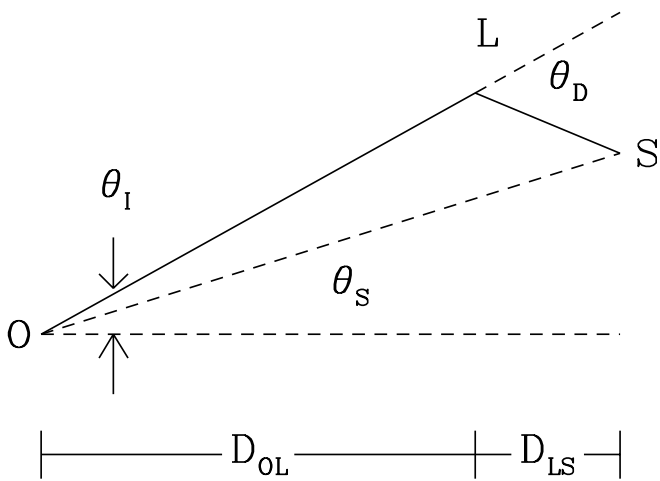


FIG. 1.—Schematic ray-tracing diagram; the solid line joining O (observer), L (lens), and S (source) represents the light ray. L represents the point of closest approach in the transiting planet's atmosphere. S represents a point on the surface of the star. The deflection is exaggerated, and the diagram is not to scale. We use the convention that θ_D has an opposite sign to θ_I and θ_S .

TABLE 1

REFRACTIVE COEFFICIENTS FOR DIFFERENT GAS COMPOSITIONS

Gas Composition	A_1 ($\times 10^5 \text{ cm}^3$)	B_1 ($\times 10^{11} \text{ cm}^{-2}$)
Hydrogen.....	13.6	7.7
Oxygen	26.63	5.07
Nitrogen	29.19	7.7
Air	28.79	5.67
Methane	42.6	14.41

NOTE.—Refractive index is $n = 1 + \alpha\rho$, with $\alpha\rho = A_1(1 + B_1/\lambda^2)$. Values are given for gases at 15°C and 1 atm of pressure.

mined by spatial gradient of the refractive index n :

$$\theta_D = - \sum \nabla n \times \Delta l \times \hat{l}, \quad (2)$$

where the sum is over individual segments of the ray Δl with \hat{l} as the unit vector and ∇ the spatial gradient.

For atmospheric lensing, $n = 1 + \alpha\rho$, where ρ is the gas density and α is a refractive coefficient that depends on both gas composition and wavelength. A common parametrization, known as Cauchy's formula, gives $\alpha\rho = A_1(1 + B_1/\lambda^2)$, where λ is the wavelength and A_1 and B_1 for common gases are given in Table 1 (Born & Wolf 1999, p. 101). For an H₂-He mixture with 24% He by mass, $\alpha = 1.243 \text{ cm}^3 \text{ g}^{-1}$ at 4400 Å, and $\alpha = 1.214 \text{ cm}^3 \text{ g}^{-1}$ at 6700 Å.

We are interested in cases in which the deflection angle is small and the lens is thin (i.e., distances over which significant deflection occurs are small compared to D_{LS} and D_{OL}). Suppose the axis connecting the observer and (the center of) the lens points in the z -direction. We have

$$\theta_D = \nabla_{\perp} \int_{-\infty}^{\infty} n dz = \nabla_{\perp} \int_{-\infty}^{\infty} \alpha\rho dz, \quad (3)$$

where ∇_{\perp} is the spatial gradient in the x - and y -directions. We use $\mathbf{b} = (b_1, b_2)$ to denote the impact vector—the vector in the (x, y) -plane from the lens center to the point of impact.

The inverse of the magnification matrix is

$$\begin{aligned} A_{ij}^{-1} &\equiv \frac{\partial \theta_S^i}{\partial \theta_I^j} \\ &= \delta_{ij} + \frac{D_{OL}D_{LS}}{D_{OL} + D_{LS}} \frac{\partial^2}{\partial b_j \partial b_i} \int_{-\infty}^{\infty} \alpha\rho dz, \end{aligned} \quad (4)$$

where we have used $\mathbf{b} = D_{OL}\theta_I$.

We are interested in a density profile ρ , which is ellipsoidal in general, in the sense that $\rho = \rho(r)$, where $r^2 = x'^2/a_1^2 + y'^2/a_2^2 + z'^2/a_3^2$. The axes denoted by x' , y' , and z' are generally not lined up with the x -, y -, and z -axes defined before. We show the following in Appendix A:

1. That such a profile is well motivated.
2. That in the simple case of an isothermal atmosphere in hydrostatic equilibrium, the density profile is $\rho(r) = \rho_0 \exp[-(r - R_0)/H]$, where R_0 is a reference radius whose

³ A spherical planet is simply a special case within the class of models we study here.

choice will be fixed below, ρ_0 is the density at R_0 , and $H = (k_B T / g \mu m_H)$ is the atmospheric scale height, where k_B is Boltzmann's constant, T is the temperature, g the surface gravity, μ the mean molecular weight, and m_H the mass of the hydrogen atom.

3. The quantity r , which we loosely refer to as “radius,” can be written as $r = [(1 - \epsilon)b_1^2 + (1 + \epsilon)b_2^2 + z^2]^{1/2}$ by a suitable rotation of axes along with rescaling of the density field—as long as the deviation from spherical symmetry is small ($\epsilon \ll 1$) or a_1, a_2 , and a_3 are not too different from each other. The projected oblateness ϵ is related to the actual oblateness of the planet $\epsilon_A \equiv (a_1 - a_3)/a_1$ (assuming that it is axially symmetric with $a_1 = a_2$) by $\epsilon = \epsilon_A(1 - \cos^2 \beta)$, where β is an Euler rotation angle;⁴ β is the angle between the axis of rotation of the planet and the line of sight (see Appendix A for details). Assuming that β is randomly distributed implies that $\epsilon = \epsilon_A/2$ on average.

We also work under the simplification that α , the density-independent refractive coefficient, is independent of position on the planet. This is a simplification because the atmospheric composition—hence the net value of α —is expected to vary with atmospheric depth.

Putting the above together and using $\nabla_\perp \rho(r) = (1 \mp \epsilon)(\mathbf{b}/r)\partial\rho/\partial r$ (upper/lower sign for b_1/b_2) in equation (2), the lensing equation (1) can be written as

$$\theta_S^1 = \theta_I^1 + (1 - \epsilon)\theta_I^1\psi(u), \quad \theta_S^2 = \theta_I^2 + (1 + \epsilon)\theta_I^2\psi(u), \quad (5)$$

where

$$\begin{aligned} \psi(u) &\equiv \alpha \frac{D_{LS} D_{OL}}{D_{OL} + D_{LS}} \int_{-\infty}^{\infty} \frac{\partial \rho}{\partial r} \frac{dz}{r}, \\ \rho &= \rho_0 \exp \frac{-(r - R_0)}{H}, \\ r^2 &= D_{OL}^2 u^2 + z^2, \\ u^2 &\equiv (1 - \epsilon)(\theta_I^1)^2 + (1 + \epsilon)(\theta_I^2)^2. \end{aligned}$$

With the above form, the problem of predicting image position(s) given a source position can be reduced to solving a simple single variable equation—this and associated computational tricks are discussed in Appendix B.

The magnification is given by (eq. [4]):

$$\begin{aligned} A \equiv \det A_{ij} &= \left[1 + 2\psi + (1 - \epsilon^2)\psi^2 + (1 - \epsilon^2)u^2\psi\tilde{\psi} \right. \\ &\quad \left. + (u^2 + \epsilon v)\tilde{\psi} \right]^{-1}, \end{aligned} \quad (6)$$

where

$$\begin{aligned} v &\equiv -(1 - \epsilon)(\theta_I^1)^2 + (1 + \epsilon)(\theta_I^2)^2, \\ u^2 &\equiv (1 - \epsilon)(\theta_I^1)^2 + (1 + \epsilon)(\theta_I^2)^2, \\ \tilde{\psi}(u) &\equiv \frac{1}{u} \frac{\partial \psi}{\partial u} = \alpha D_{OL}^2 \frac{D_{OL} D_{LS}}{D_{OL} + D_{LS}} \int_{-\infty}^{\infty} \left(\frac{1}{r^2} \frac{\partial^2 \rho}{\partial r^2} - \frac{1}{r^3} \frac{\partial \rho}{\partial r} \right) dz, \end{aligned}$$

and where u , ψ , and ρ are as described in equation (5). The caustic is defined by source positions where A diverges. The critical curve is the image of the caustic. We discuss in Appendix B how to find both, if they exist—a situation referred to as strong lensing.

⁴ In this paper, we use the terms oblateness and ellipticity interchangeably.

Finally, the observed flux from a star during an extrasolar planet transit is given by

$$F(t) = \int d^2\theta_S \sum AI[\theta_S - \theta_*(t)]W(\theta_I), \quad (7)$$

where $I[\theta_S - \theta_*(t)]$ is the surface brightness of the star as a function of source position. The symbol $\theta_*(t)$ denotes the position of the star's center as a function of time. We have chosen the origin of θ_S and θ_I to be centered at the planet. The sum is over all images for a given source position. The kernel $W(\theta_I)$ describes the occultation and absorption; in this paper, we focus on a simple model in which $W(\theta_I)$ is a step function,

$$W(\theta_I) = \begin{cases} 1, & \text{if } \sqrt{(1 - \epsilon)(\theta_I^1)^2 + (1 + \epsilon)(\theta_I^2)^2} > \frac{R_0}{D_{OL}}, \\ 0, & \text{otherwise.} \end{cases} \quad (8)$$

This step function specifies R_0 . It is the (elliptic) radius below which the projected density exceeds some value such that the atmosphere becomes completely opaque or it is the radius at the rocky surface of a planet. A more realistic treatment of absorption will have W changing more gradually than this step function and also changing with wavelength; this will be discussed in § 6. As we will see, our step function model is actually a good approximation to reality. Note that both I and A above are functions of wavelength. Finally, for most purposes, we are only interested in the normalized $F(t)$, i.e., $F(t)$ (eq. [7]) divided by its asymptotic value well away from the transit—the stellar flux: $\int d^2\theta_S I(\theta_S)$. From now on we use $F(t)$ to refer to the normalized value, and whenever we refer to “flux” in this paper, we always mean the stellar flux normalized by its pre- or posttransit value.

To summarize, equations (5), (6), and (7) completely specify the problem of atmospheric lensing during a planetary transit for an isothermal atmosphere in hydrostatic equilibrium with an ellipsoidal density profile.

2.2. Atmospheric versus Gravitational Lensing

Gravitational lensing can be described by essentially the same equations presented above except that the refractive index n in equation (3) is equal to $1 - 2\phi$, where ϕ is the gravitational potential instead of $1 + \alpha\rho$. That α is wavelength-dependent implies that atmospheric lensing is color-dependent, whereas gravitational lensing is achromatic.

Similarly, gravitational lensing by an elliptic potential obeys equations (5), (6), and (7) with $\alpha\rho$ replaced by -2ϕ . It is interesting to note, however, that a well-known theorem in gravitational lensing, the magnification theorem, does not hold in atmospheric lensing. The magnification theorem states that for a given source position, the magnification of all images must sum to at least unity. This can be traced back to the fact that $\nabla^2\phi$ is proportional to the mass density, which is positive definite. For atmospheric density, the relevant quantity $\nabla^2\rho$ is not guaranteed to be positive definite. In other words, in atmospheric lensing the magnification need not sum to unity, and thus a net suppression of flux can occur.

Another important difference between gravitational and atmospheric lensing is that gravitational lensing is almost never significant when the lens is very close to the source or the observer. This arises from the fact that the combination

of distances $D_{LS}D_{OL}/(D_{OL} + D_{LS})$ becomes small (dominated by the smaller of the two distances) if $D_{LS} \ll D_{OL}$ or $D_{OL} \ll D_{LS}$. While the same factor applies to both types of lensing, atmospheric lensing has the advantage of having available an exponential density field (or nearly so; see Appendix A). The analog for gravitational lensing, an exponential potential, almost never occurs in nature; power-law falloff is far more prevalent. An exponential density profile allows large gradients to offset an unfavorable combination of distances. To be more precise, while a power-law profile would result in factors of $D_{LS}D_{OL}/[(D_{OL} + D_{LS})R_0]$ in the relevant expressions [e.g., $\psi(u)$ in eq. (5)], an exponential profile gives $D_{LS}D_{OL}/[(D_{OL} + D_{LS})H]$, which is considerably larger (because atmospheric scale height $H \ll R_0$, where R_0 is the planet radius). Nature offers a nice existence proof: atmospheric lensing of distant stars by the solar system planets has been observed in spite of the fact that $D_{OL} \ll D_{LS}$ (see § 4.3). The extrasolar case we are interested in can be viewed as the symmetrical opposite with $D_{LS} \ll D_{OL}$.

3. PARAMETER ACCOUNTING

Several parameters enter into the problem of planetary atmospheric refraction during a transit. However, most of them appear in a few combinations. It is helpful to list them explicitly.

The quantities $\psi(u)$ and $u^2\tilde{\psi}(u)$ in the lens mapping equation (5) can be well approximated by the following expressions if $uD_{OL}/H \gg 1$. This is true in realistic cases because uD_{OL} is constrained to be larger than R_0 in order for an image not to be obscured (occulted or absorbed) by the planet.

$$\begin{aligned} \psi(u) &= -B\sqrt{\pi/2} \left(\frac{uD_{OL}}{H}\right)^{-1/2} \exp\left[-\frac{uD_{OL} - R_0}{H}\right], \\ u^2\tilde{\psi}(u) &= B\sqrt{\pi/2} (uD_{OL}/H)^{1/2} \left[1 + \left(\frac{uD_{OL}}{H}\right)^{-1}\right] \\ &\quad \times \exp\left[-\frac{(uD_{OL} - R_0)}{H}\right], \\ B &\equiv 2\alpha \frac{\rho_0}{H} \frac{D_{LS}D_{OL}}{D_{OL} + D_{LS}}. \end{aligned} \quad (9)$$

Note that refraction is important (or the magnification A is significantly different from unity) only if uD_{OL} is close to R_0 . Therefore, as far as the gross lensing behavior (or lack thereof) is concerned, only three parameters are important, B as defined above, R_0/H , and ϵ .

The parameter R_0/H is a measure of the relative importance of the binding energy and the thermal energy of the atmosphere. The quantity B can be understood as the deflection angle scaled by ratios of distances—to be more precise, $B = 2(D_{LS}/H)[(2\pi R_0/H)^{1/2}]^{-1}\theta_D$, where θ_D is the deflection angle (i.e., $\alpha\rho_0 = [(2\pi R_0/H)^{1/2}]^{-1}\theta_D$). Note that D_{LS} is replaced by D_{OL} if $D_{OL} \ll D_{LS}$, such as for the lensing of distant stars by solar system planets. It is important to emphasize that ρ_0 here is the density at which the atmosphere starts to become transparent (i.e., optical depth unity) or, equivalently, θ_D is the deflection angle at an impact parameter corresponding to unit optical depth (see § 6).

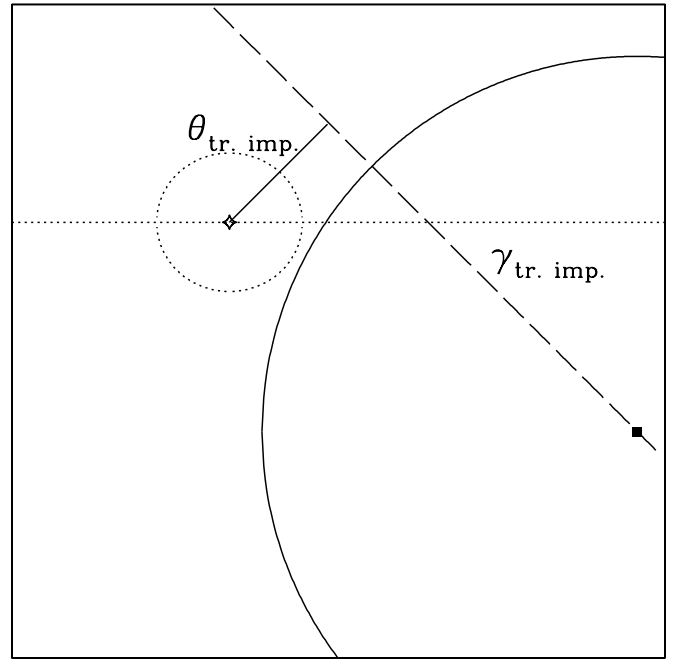


Fig. 2.—Geometrical set up of a planetary transit. The circular solid line represents the boundary of the star, while the ellipsoidal dotted line represents that of the planet. The filled square is the center of the star, which moves along the dashed line with respect to the planet. The horizontal dotted line defines the major axis of the planet; $\gamma_{\text{tr imp}}$ is the angle between the horizontal and dashed line, while $\theta_{\text{tr imp}}$ is the distance in angular units of closest approach between the planet center and the stellar center.

In addition to the three lensing parameters, we have three transit parameters. They are the transit impact parameter (as opposed to the *lensing* impact parameter) $\theta_{\text{tr imp}}$ (the distance of closest approach between the center of the planet and the center of the star in angular units),⁵ the transit impact angle $\gamma_{\text{tr imp}}$ (the angle between the projected planetary ellipse and the direction of transit motion), and the transit velocity w in angular units per unit time. See Figure 2 for an illustration. Since w basically rescales the time axis in our prediction of the transit light curve, we do not treat it as a free parameter in our predictions. We estimate it by using $w = (GM_{\odot}/D_{LS})^{1/2}/D_{OL}$.

Finally, there are the parameters that describe the star: the stellar radius R_* and the surface brightness of the star, or its limb-darkening function, which is often parametrized as

$$\begin{aligned} I(\theta_S - \theta_*) &= 1 - u_*(1 - s) \\ &\quad - v_*(1 - s^2) \text{ if } |\theta_S - \theta_*|D_{OL} \leq R_*, \\ I(\theta_S - \theta_*) &= 0 \text{ otherwise,} \end{aligned} \quad (10)$$

where

$$s \equiv \sqrt{1 - \left(\frac{|\theta_S - \theta_*|D_{OL}}{R_*}\right)^2},$$

and where θ_* is the angular position of the star's center (recall that we have chosen the origin to be at the center of

⁵ The parameter $\theta_{\text{tr imp}}$ is related to the planet orbital inclination i by $\theta_{\text{tr imp}} = [D_{LS}/D_{OL}] \cos i$.

the lens, the planet). The limb-darkening parameters u_* and v_* are generally wavelength-dependent. Typical values are $u_* = 0.8$ and $v_* = -0.225$ in red bands, $u_* = 0.99$ and $v_* = -0.17$ in blue bands, and $u_* = 0.93$ and $v_* = -0.23$ in intermediate yellow bands (Cox 2000). Clearly, as far as the gross features of the transit are concerned, it is the ratio R_*/R_0 that is important, not the absolute size of R_* (other than a rescaling in the overall duration of the transit).

In summary, we have three lensing parameters, ϵ , B , and R_0/H , two transit parameters, $\theta_{\text{tr imp}}$ and $\gamma_{\text{tr imp}}$, and three stellar parameters, R_*/R_0 , u_* , and v_* . In the case of a spherical planet, the total number of parameters is reduced by two because the lensing parameter ϵ and the transit parameter $\gamma_{\text{tr imp}}$ are not needed. We will not perform an exhaustive study of the full parameter space in this paper but will be content with a mostly qualitative (with a few exceptions) description of the dependence of the transit light curve on these parameters. Some of these parameters are likely degenerate. For instance, changing $\theta_{\text{tr imp}}$ means that the transit is sampling a different part of the stellar profile, which might be mimicked by a different limb-darkening law (e.g., a different u_* and v_*). Finally, note that for extrasolar systems, $D_{OL} \gg D_{LS}$, and so D_{OL} drops out of the lensing equation (see, e.g., eq. [5]) and appears only as an unobservable overall scaling of angular separations.

4. STRONG LENSING AND CAUSTIC STRUCTURE

4.1. Condition for Strong Lensing

The first question we would like to address is when strong lensing—i.e., the existence of caustics or multiple images (which may be unresolved)—occurs. The existence of caustics could lead to significant modifications in transit light curves.

Caustics in the source plane, or critical curves in the image plane, can be obtained by solving for divergent magnification, $A^{-1} = 0$ (eq. [6]). In the spherical case, with $\epsilon = 0$, this is straightforward. Recall that images must have $u > R_0/D_{OL}$ to be visible; otherwise, they are blocked (occulted or absorbed) by the planet (eq. [8]). Therefore, the condition for strong atmospheric lensing by a spherical planet is

$$\begin{aligned} 1 + 2\psi(u) + \psi(u)^2 + u^2\psi(u)\tilde{\psi}(u) + u^2\tilde{\psi}(u) \\ = [1 + \psi(u)][1 + \psi(u) + u^2\tilde{\psi}(u)] < 0, \\ u = \frac{R_0}{D_{OL}}. \end{aligned} \quad (11)$$

This guarantees that some images with $u > R_0/D_{OL}$ will have $A^{-1} = 0$. Using the results in § 3, the above condition imposes a relation between only two parameters: B and R_0/H .

Since ϵ is small, the condition for strong lensing by an elliptic atmosphere will not be too different from the spherical case described above. We estimate it using results proved in Appendix B (eq. [B5] and the following paragraph), replacing the above condition with the following

$$\begin{aligned} 1 + 2\psi(u) + (1 - \epsilon^2)\psi(u)^2 + (1 - \epsilon^2)u^2\psi(u)\tilde{\psi}(u) \\ + (1 - \epsilon)u^2\tilde{\psi}(u) < 0, \\ u = \frac{R_0}{D_{OL}}. \end{aligned} \quad (12)$$

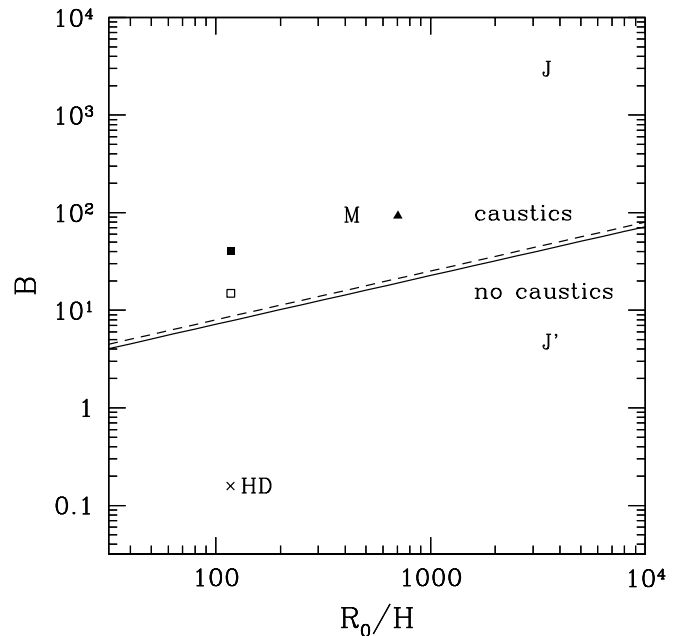


FIG. 3.—Separation of the strong lensing regime (existence of caustics) from the weak lensing regime for the combination of parameters B and R_0/H (delineated by solid and dashed lines). The solid line is for projected oblateness/ellipticity $\epsilon = 0.1$, and the dashed line is for a sphere, $\epsilon = 0$. The parameter B is defined as $B = 2\alpha(\rho_0/H)D_{LS}D_{OL}/(D_{OL} + D_{LS})$ (eq. [9]). The quantity R_0/H is the ratio of planet radius to atmospheric scale height. We show values of B and R_0/H for HD 209458b (HD), where $D_{LS} \ll D_{OL}$, and for Mars (M) and Jupiter (J), where $D_{LS} \gg D_{OL}$. In all cases, observations at optical wave bands are assumed. We show with the symbol J' the parameters for Jupiter if it were observed at wave bands with 600 times stronger absorption (e.g., in the UV; see text for details). The filled square denotes the fiducial model we study in this paper. The triangle, open square, and cross are other models we also discuss.

Using equation (9), this imposes a condition on three parameters, ϵ , B , and R_0/H ,

$$1 - \sqrt{\frac{\pi}{2}} \sqrt{\frac{H}{R_0}} B - \epsilon < 0, \quad (13)$$

where we have used $H/R_0 \ll 1$ and $\epsilon \ll 1$. This is a main result of our paper.

The above condition for strong lensing is depicted in Figure 3. We show in the same figure the relevant parameters for several known planets. We assume $\alpha = 1.2 \text{ cm}^3 \text{ g}^{-1}$ for all of them. Mars (M) has $R_0 \sim 3400 \text{ km}$, $D_{OL}D_{LS}/(D_{OL} + D_{LS}) \sim 1.5 \text{ AU}$, $\rho_0 \sim 1.5 \times 10^{-6} \text{ g cm}^{-3}$, and $H \sim 8.7 \text{ km}$ (Jones 1999 p. 314). Jupiter (J) has $R_0 \sim 71,000 \text{ km}$, $D_{OL}D_{LS}/(D_{OL} + D_{LS}) \sim 5.2 \text{ AU}$, $\rho_0 \sim 3.5 \times 10^{-5} \text{ g cm}^{-3}$, and $H \sim 21.7 \text{ km}$ (Jones 1999 p. 341). The extrasolar planet HD 209458b (HD) has $R_0 \sim 10^5 \text{ km}$, $D_{OL}D_{LS}/(D_{OL} + D_{LS}) \sim 0.05 \text{ AU}$, $\rho_0 \sim (1-6) \times 10^{-6} \text{ g cm}^{-3}$, and $H \sim 500-700 \text{ km}$ (Charbonneau et al. 2000; Henry et al. 2000; Mazeh et al. 2000; Jha et al. 2000; Burrows et al. 2000). The density ρ_0 is obtained by computing the density at which the optical depth for Rayleigh scattering is unity (at $\lambda = 6500 \text{ \AA}$; see § 6),⁶ or in the case of Mars, ρ_0 is the density at the base of its atmosphere, just above its

⁶ The amount of absorption assumed here can be regarded as an absolute minimum. Additional absorption due to, for instance, clouds or water molecules will decrease ρ_0 and therefore B (see Hubbard et al. 2001). The fact that our assumed (optimistic) B still fails to meet the strong lensing criterion implies that caustics can be safely ignored in the case of HD 209458b.

solid surface. For a gaseous planet or a rocky planet with a thick atmosphere, ρ_0 (and R_0) is wavelength-dependent. For example, our own solar system planets have much stronger molecular absorption in the UV and IR compared to the optical. Strong absorption bands make ρ_0 smaller (where, again, ρ_0 is the density and R_0 the radius at which the optical depth equals 1), in some cases to the point where atmospheric lensing is no longer strong (recall that $B \propto \rho_0$). This is illustrated by the point *J*, where we show Jupiter observed at a wave band where the absorption cross section is 600 times larger, e.g., Rayleigh scattering observed at $\lambda = 1300 \text{ \AA}$ instead of 6500 \AA . The main effect is a dramatic decrease in B . The increase in R_0/H is very small because the radius varies only logarithmically with the density. We will discuss the color dependence of lensing in more detail in § 6.

There is clearly a wide range of possibilities in the two-dimensional parameter space of B and R_0/H . Recall that $B \equiv 2\alpha(\rho_0/H)[D_{LS}D_{OL}/(D_{OL} + D_{LS})]$; thus, B depends on many parameters of the planetary system. For example, B depends on the planetary atmosphere through H , which can depend strongly on stellar type and orbital distance via heating, through ρ_0 , which is very sensitive to the presence of optically thick clouds, and through α . *J* and HD, which have a similar mass, occupy very different parts of the B versus R_0/H diagram primarily because they are situated at very different distances from their parent stars. Higher temperature in the latter leads to a much larger atmospheric scale height. To investigate how variables such as stellar luminosity, albedo, planet mass, and composition control the lensing behavior is outside the scope of this paper. In fact, the radial velocity detections of extrasolar planets have taught us that planet orbital characteristics can be quite different from expectations based on the solar system. We therefore adopt the philosophy that the parameters spanned by three examples (shown by the open square, cross, and triangle in Fig. 3) are all possible and interesting, and our goal is to understand the importance of atmospheric lensing under these conditions. We will briefly discuss the physical motivations for the choice of some parameters in § 7.

4.2. Caustic Structure and Magnification

The lower panel of Figure 4 shows the caustic (solid line) and the critical curve (dotted line) for a fiducial model with projected oblateness $\epsilon = 0.05$ denoted by the filled square in Figure 3 (see § 5 for details). A point source situated within the caustic produces four images.⁷

The upper panel of Figure 4 shows the magnification as a function of source position for a point source situated on the x -axis. This figure shows that lensing has two effects. First, it suppresses the flux originating from source positions just outside R_0 ($uD_{OL} > R_0$). Second, it brings in additional photons from source positions behind R_0 ($uD_{OL} < R_0$)—photons that would otherwise be blocked (occulted or absorbed) by the planet. Which effect dominates can be calculated by integrating over the star

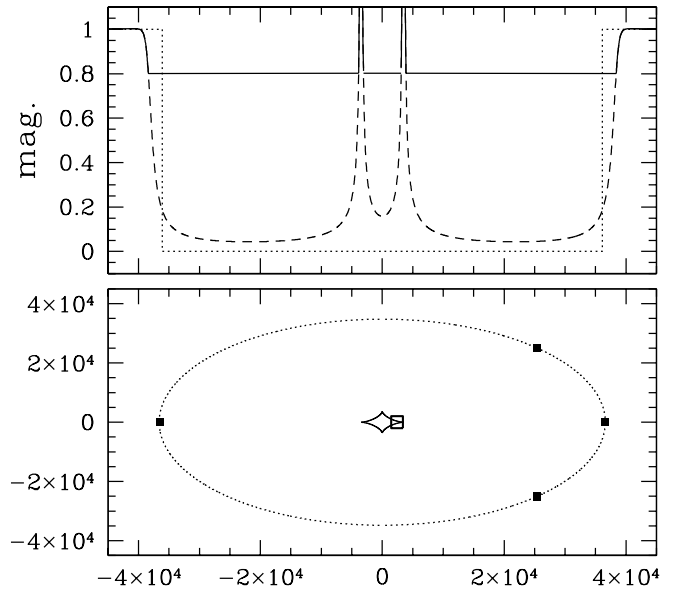


FIG. 4.—*Top*: Magnification as a function of source position for source positions (dashed line; overlaps with solid line in the upper portion) that lie on the major axis of the planet (the x -axis in the lower panel). The dotted line shows the occultation kernel W as defined in eq. (8). The solid line represents the light curve for an occultation by a solar system planet of a distant star, which happens to be moving along the planet's semimajor axis. See text for details. *Bottom*: Caustic, source positions where the magnification diverges (solid line), while the dotted line shows the critical curve, which is the image of the caustic. The four filled squares are images of a point source denoted by an open square situated just inside the caustic. The axis coordinates are distances (in kilometers) in the lens plane; i.e., they correspond to physical distances from the planet center.

(regarded here as a collection of point sources) and depends on details of the magnification profile and the limb-darkening profile (i.e., the lensing parameters, transit parameters, and stellar parameters described in § 3). We can derive a simple result from equation (7) for the limiting case of a completely flat and constant I . Taking I out of the integral in equation (7), F can be rewritten as $I \int d^2\theta_I W(\theta_I)$, which is identical to the result if no lensing takes place. It is not hard to see that the same conclusion follows if I is constant within some region and if the planet is well within this region. In other words, if there is strictly no limb darkening, there will be no net gain or loss of stellar flux from atmospheric lensing, provided that the projected planet is well within the stellar disk.

Realistic stellar profiles are never exactly constant. Refraction therefore generally modifies the dimming or deficit of the stellar flux during a transit, especially during ingress and egress. The sign of the modification depends on the exact transit and lensing parameters. The size of the modification can be crudely estimated from the ratio of the projected area of the atmosphere to that of the planet: $\sim H/R_0$ if strong lensing occurs.

4.3. Application to Solar System Occultations

Figure 4 also represents an occultation of a point-source background star by a solar system planet. The dotted line shows what one would expect for an atmosphereless planet (ignoring diffraction): the stellar intensity is constant and vanishes instantaneously when the star passes behind the planet as viewed by the observer. The dashed line shows the magnification from equation (6) when refraction by the at-

⁷ It is interesting to note that lensing by an elliptic potential or density profile generally produces two sets of caustic curves (see, e.g., Schneider et al. 1992), whereas we see only one here. The origin can be traced to the fact that $\psi(u)$ in eq. (5), which is proportional to the deflection angle, is monotonic. We do not expect small local deviations from the exponential density profile to change this conclusion because $\psi(u)$ involves an integral over many layers of the atmosphere.

mosphere is significant. The magnification curve can be understood qualitatively as follows: (1) The diminution of starlight during ingress and egress is due to atmospheric differential refraction (not by absorption that occurs at much lower depths in this model), which causes stellar light rays to diverge away from the planet-observer line of sight. This is a consequence of the radial density gradient in the atmosphere. (2) When the star is behind the opaque part of the planet, the occultation light curve is not zero because some of the stellar light rays are refracted into the observer's line of sight. (3) When the point source is near the geometric center of the planet, the stellar flux is symmetrically refractively focused, causing an increase in brightness. The solid line in Figure 4 shows the occultation light curve that includes the flux from the planet from reflected sunlight if the occulted star has an intensity 20% of the planet. The solid curve shows that the planet's reflected light dominates the light curve during the stellar occultation. Hence the minimum observed brightness corresponds to the planet alone, and the full extent of refractive focusing and defocusing is not observed for bright solar system planet occultations of background stars. The magnification peaks have been observed for most solar system planets (and with the multiple images even resolved in the case of Saturn; see Nicholson, McGhee, & French 1995). Note that the magnification peaks are generally reduced because of atmospheric absorption or scattering and to the finite size of the star. Note also that if the star does not move along the axes of symmetry of the solar system planet, the two magnification peaks will generally be of different heights and widths. Also, the two peaks will merge into one if the planet's oblateness is sufficiently small. Refractive occultations of all of the solar system planets (except Mercury) have been observed and in some cases well studied (see Elliot & Olkin 1996 and references therein). Models of them can provide temperature (T), pressure (P), and density (ρ) as a function of atmospheric depth.

5. THE TRANSIT LIGHT CURVE

5.1. Exploring the R_0/H - B Plane

Figure 5 shows the transit light curve with or without lensing for a fiducial model denoted by the filled square in Figure 3: $B = 40.3$, $R_0/H = 117.3$, and $\epsilon = 0.05$, together with $R_0/R_* = 0.084$, $R_*/(GM_\odot/D_{LS})^{1/2} = 233.66$ minutes, $u_* = 0.8$, $v_* = -0.225$, $\theta_{\text{tr imp}} = 2R_0/D_{OL}$, and $\gamma_{\text{tr imp}} = 45^\circ$. Because B depends on several parameters including planetary scale height and orbital distance, the fiducial model can be realized by several different kinds of planetary systems (e.g., different star types and orbital distances). Although the fiducial model is not intended to represent any planet in particular, a physical realization of the fiducial model is described in § 7. The last six parameters define the overall light deficit and rough duration of transit, the limb-darkening profile, and the geometry of the transit. We emphasize that a different value for $R_*/(GM_\odot/D_{LS})^{1/2}$ (§ 3) can be easily accommodated by rescaling the time axis of all light curves shown below.

To better isolate the effect of lensing, we define and show in Figure 6 the following quantity (*solid line*):

$$f(t) = \frac{\Delta F_{\text{lens}}(t) - \Delta F_{\text{no lens}}(t)}{\Delta F_{\text{lens}}^{\text{max}}}, \quad (14)$$

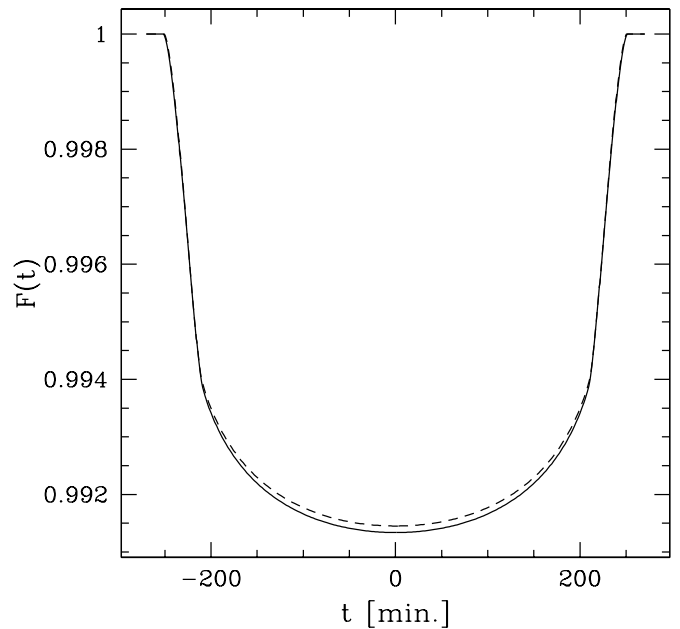


FIG. 5.—Transit light curve for our fiducial model (denoted by a filled square in Fig. 3) with atmospheric lensing (*solid curve*) and without (*dashed curve*). $F(t)$ is the normalized stellar flux (eq. [7]). The star here has $R_* = 0.6 R_\odot$.

where $\Delta F(t) \equiv 1 - F(t)$ represents the light deficit and the subscripts denote whether or not lensing is taken into account (with all other parameters fixed). We choose to normalize by the maximum deficit, which can be estimated

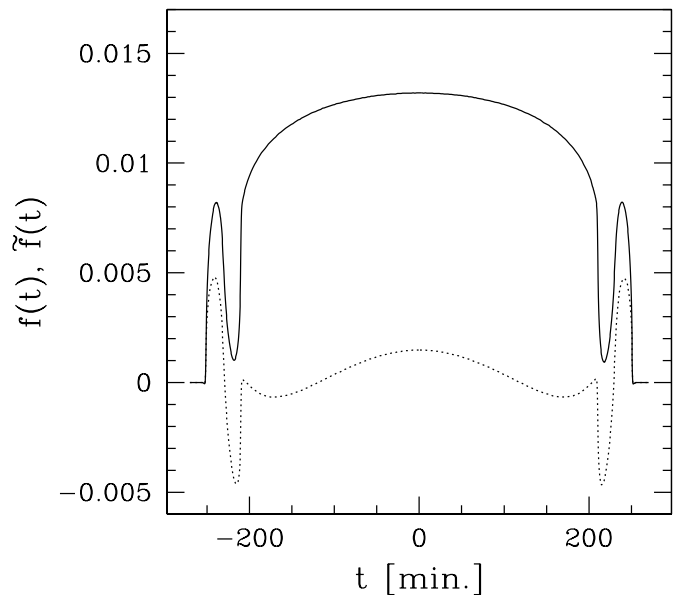


FIG. 6.—Fractional difference between the flux deficit from a stellar light curve, $f(t)$, with and without planetary atmospheric lensing (*solid line*; eq. [14]). This is for the fiducial model denoted by the filled square in Fig. 3. The dotted line shows $\tilde{f}(t)$ as defined in eq. (15), the fractional difference between the light deficit from a lensed fiducial model and an unlensed model with parameters of the unlensed model tuned to minimize this fractional difference: $R_0 = 35,400$ km, $H = 300$ km, $R_* = 417,600$ km, $u_* = 0.832$, $v_* = -0.2475$, $\rho_0 = 1.68 \times 10^{-5}$, $\epsilon = 0.05$, $w = 2.9741 \times 10^{-13}$ s $^{-1}$, $\gamma_{\text{tr imp}} = 49^\circ 5$, and $\theta_{\text{tr imp}} = 69,696$ km/ D_{OL} .

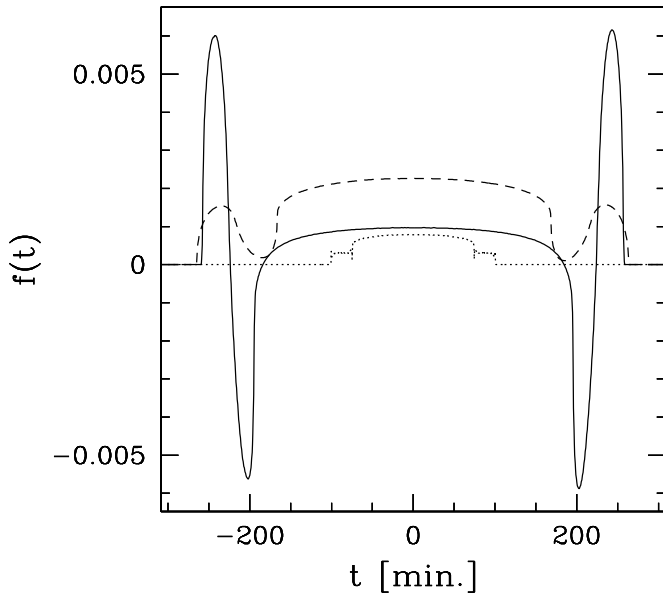


FIG. 7.—The $f(t)$ (eq. [14]) for three different planetary models corresponding to the open square (solid line), cross (dotted line), and triangle (dashed line) in Fig. 3. Parameters for the dotted line resemble those for HD 209458b.

roughly by $(R_0/R_*)^2$.⁸ The quantity f is therefore a *fractional* difference. This gives us a nice way to estimate the *absolute* size of the deficit for a transit with any given R_0/R_* : it is roughly $(R_0/R_*)^2(1+f)$. As we have discussed in § 4, f can be estimated by $\sim H/R_0$, which is around 1% for our fiducial model. This is in rough agreement with the results of our numerical integration. The *absolute* change in flux due to lensing is therefore $1\% \times (R_0/R_*)^2$, which for the example shown with $R_0/R_* \sim 0.1$, is 10^{-4} —a potentially significant effect.

The solid line in Figure 7 shows the same quantity f for a transiting planet with the same H/R_0 but a smaller B ($=14.9$)—denoted by an open square in Figure 3. The overall magnitude of f is a little smaller but not too dissimilar from the fiducial model above. The sign of the lensing effect as the transit progresses, however, is quite different. As we have previously discussed, two opposing lensing effects are competing. One is the suppression of flux from source positions just above R_0 . The other is the addition of photons from source positions in the planet’s shadow. For the model with a larger B , the first dominates over the second effect at all times. For the model here with a smaller B , the second effect dominates, at least temporarily toward the end of ingress or beginning of egress. At midtransit, however, the first effect still dominates. Interestingly, a search through a whole range of limb-darkening parameters reveals that lensing almost always causes a net suppression of flux at midtransit except when the stellar profile is very spiky at the center.

When B is decreased further so that caustics no longer exist, the first effect, suppression of flux, will dominate. This is illustrated by the dotted line in Figure 7, which is the model denoted by a cross in Figure 3, and is chosen to

⁸ We could normalize by the maximum deficit in the nonlensed case, but it would only modify $f(t)$ to higher order ($O[f(t)^2]$).

resemble HD 209458b (see § 4.1).⁹ Clearly, atmospheric lensing is weak for the close-in extrasolar giant planets like HD 209458b. This is no surprise since, as we have pointed out in § 4.1 and Figure 3, there are no caustics in the case of HD 209458b. This is due to the low B , which is mainly caused by a small lens-source distance because B is proportional to D_{LS} . A second, less direct effect of the small D_{LS} is that the planet’s temperature is hotter, and thus H is higher, further decreasing B . However, it is interesting that even though the combination of parameters does not allow the existence of caustics in the case of HD 209458b, refraction nonetheless could modify the light curve at a (fractional) level of $\sim 5 \times 10^{-4}$ (depending on the actual atmospheric structure; see § 7 for details). Note also that because $D_{LS} = 0.05$ AU for this close-in gas giant (compared to $D_{LS} = 1$ AU we adopt in previous cases), the shorter orbital radius leads to a higher velocity (the parameter w ; see § 3), hence, a shorter transit. Finally, the dashed line in Figure 7, $f(t)$, shows the model shown by a triangle in Figure 3. The behavior is similar to the solid line of Figure 6 except that the overall effect is weaker. This is due to a larger R_0/H , ~ 700 , from which one expects f on the order of $\sim 1.5 \times 10^{-3}$, in agreement with what we find.

5.2. The Lensing Signal

The previous section shows that lensing can modify the transit light curve to an extent that is potentially detectable in some cases. If so, high-precision photometric observations of extrasolar planet transits can provide planet atmosphere parameters such as scale height and density, both of which affect the lensing behavior. What is not clear, however, is whether a transit light curve from a planet with lensing can be distinguished from a transit light curve from a planet with slightly different parameters but with no lensing. This is what we investigate here.

As shown in the last section, the modification introduced by atmospheric lensing is qualitatively quite different for models with or without caustics. For models with caustics, such as those shown in Figure 6, $f(t)$ experiences a significant dip in the light deficit around ingress and egress (the same holds for solid and dashed lines in Fig. 7). This dip is caused by the additional photons brought in from the planet’s shadow because of lensing, which causes the light deficit to drop temporarily. In other words, the inexorable dimming of starlight at ingress is temporarily slowed down by the additional photons that are refracted into view. This effect is much weakened if caustics do not exist, as in the case of the dotted line in Figure 7, which is our model for HD 209458b. This dip, or slight reduction in the rate of dimming, introduces a distinct shape to the transit light curve during ingress and egress, which one might hope to observe.

The dotted line in Figure 6 shows the following fractional difference:

$$\tilde{f}(t) = \frac{\Delta F_{\text{lens}}(t, P) - \Delta F_{\text{no lens}}(t, P')}{\Delta F_{\text{lens}}^{\text{max}}(P)}, \quad (15)$$

where the extra argument P denotes the whole set of param-

⁹ The projected ellipticity is chosen to be 10^{-3} , although its precise magnitude does not affect our conclusions here. The small oblateness is expected to be due to the tidal locking of rotational and orbital motions given the proximity of HD 209458b to its companion star (see Seager & Hui 2002a).

eters that determine the transit characteristics. We use P' for the second term (which does not take into account lensing) to emphasize that the second term has a different set of parameters from the first term. The question is how small one can make \tilde{f} by choosing P' appropriately. If $\tilde{f}(t)$ is too small to be detectable, then for practical purposes, one cannot tell from the observed light curve whether or not refraction plays a role and therefore cannot determine useful parameters from refraction effects.

The dotted line in Figure 6 shows the result of our effort of searching for the appropriate $\Delta F_{\text{no lens}}(t, P')$ that would minimize $\tilde{f}(t)$ for our fiducial model (filled square in Fig. 3). We systematically vary a host of parameters, including R_0 , u_* , v_* , w , $\theta_{\text{tr imp}}$, and $\gamma_{\text{tr imp}}$. The minimum fractional difference we can come up with is a model that brings $\tilde{f}(t)$ down to about 10^{-3} during midtransit but still almost 5×10^{-3} at ingress and egress. It should be emphasized, however, that it is conceivable that a different limb-darkening law from the one we have adopted (eq. [10]) could be chosen to further decrease \tilde{f} . Nonetheless, within the range of simple models we consider, it appears that the lensing signal (i.e., the caustic signal) cannot be completely masked by a clever choice of parameters. A discrepancy in \tilde{f} of 5×10^{-3} is potentially observable; this *fractional* difference of 5×10^{-3} means, for a transit where, say, $R_0^2/R_*^2 \sim 10^{-2}$ the *absolute* difference in the light deficit would be $\sim 0.5 \times 10^{-4}$. We will discuss other nonlensing effects that might be of similar magnitude in § 7.

We find that the same conclusion holds for other cases with caustics, such as those shown as solid and dashed lines in Figure 7. For cases without caustics, on the other hand, such as that shown with a dotted line in Figure 7, we find that a suitable choice of R_0 for the second term in equation (15) is generally sufficient to make \tilde{f} quite small and undetectable.

The time derivative dF/dt provides another way to illustrate the effect of refraction. Figure 8 shows the time derivative dF/dt for our fiducial model, with (*solid line*) or without (*dotted line*) lensing. The bottom panel focuses on the part of ingress where dF/dt reaches its minimum value before

increasing. This corresponds roughly to when half of the planet has crossed the stellar limb. What is interesting is that the presence of caustics introduces a distinct enhancement in dF/dt (*solid over dotted curve*) around $t = -230$ minutes. This is due to the additional photons brought about by the caustic. From Figure 4 we can see that the caustic has a size of about $0.2R_0/D_{OL}$. Dividing it by w , the angular velocity, we obtain ~ 5 minutes, in rough agreement with the duration of the enhancement seen in Figure 8. Since the size of the caustic scales with ϵ , this offers a direct way of measuring the projected oblateness of the planet. However, it appears that one needs to be able to detect differences in dF/dt at the level of at least one part per million per minute, which is likely difficult to achieve in the near future. Therefore, while the derivative dF/dt offers an interesting way to look at the effect of lensing, the integral fractional differences \tilde{f} or f might be a more practical probe.

5.3. The Oblateness Signal

The projected oblateness or ellipticity of a planet can affect the transit light curve. Here we explore the fractional difference

$$f_e(t) = \frac{\Delta F(t, \epsilon = 0.1) - \Delta F(t, \epsilon = 0)}{\Delta F^{\text{max}}(\epsilon = 0.1)} \quad (16)$$

to determine the magnitude of the effect. Here ΔF can either have lensing taken into account or not because we would like to investigate how oblateness affects the light curve irrespective of whether or not refraction is present. Figure 9 shows f_e for the fiducial model (filled square in Fig. 3). The solid line denotes a case with lensing and the dotted line without. It is interesting that oblateness introduces a modification to the light curve that is quite similar in the two cases.

Next we pursue the same exercise as before and ask if parameters P' can be found such that the following can be

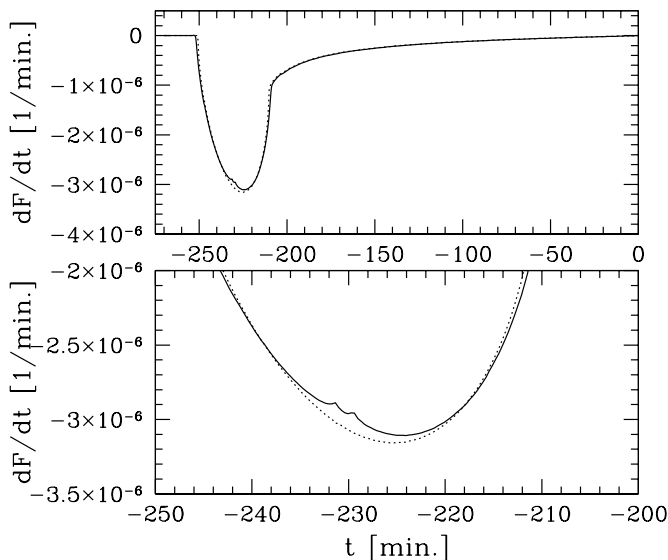


FIG. 8.—The dF/dt for the fiducial model with $\epsilon = 0.05$, denoted by the filled square in Fig. 3. The lower panel is a magnified version of the upper one. The solid line is with lensing, and the dotted line is without.

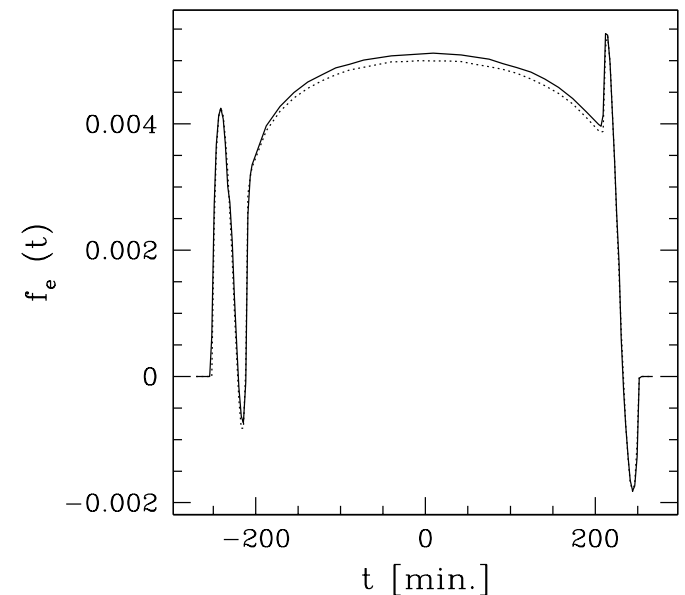


FIG. 9.—Fractional difference between the light deficit from a transit of an elliptical planet and a spherical planet, f_e , for the fiducial model denoted by the filled square in Fig. 3. The solid line is for a transit with lensing and the dotted line for a transit without.

minimized:

$$\tilde{f}_e(t) = \frac{\Delta F(t, \epsilon = 0.1, P) - \Delta F(t, \epsilon = 0, P')}{\Delta F^{\max}(\epsilon = 0.1, P)}, \quad (17)$$

where P denotes the parameters for our fiducial model. Figure 10 shows the results. We cannot find combinations of parameters P' to reduce \tilde{f}_e below 10^{-3} at ingress and egress, suggesting that we might be able to distinguish light curves caused by ellipsoidal versus spherical planets. The P' that minimizes \tilde{f}_e , as shown in Figure 10, turns out to correspond to a spherical planet with slightly larger R_0 and essentially the same area as the ellipse in the fiducial model. In other words, the curves in Figure 10 basically show the fractional difference between the light deficit of a spherical planet and an oblate planet ($\epsilon = 0.1$) with the same area (with or without lensing). This is a detectable signature.

How large is the lensing signature compared to the oblateness signature for the same stellar parameters? For our fiducial planet model, a comparison between Figure 6 and (the dotted line of) Figure 10 shows that the two effects are of a comparable magnitude. Note, however, the oblateness signature can persist even if the parameters are not right for strong lensing.

The reader might have noticed that some of the previous light curves are not symmetric around $t = 0$ (which is chosen to be the point of midtransit or minimum flux). This is due to the fact that the major/minor axis of the planet is misaligned with the direction of motion (see Fig. 2); i.e., only $\gamma_{\text{tr imp}} = 0$ or $\gamma_{\text{tr imp}} = 90^\circ$ would produce a light curve that is symmetric around $t = 0$. In the presence of a general misalignment, the asymmetry provides another useful diagnostic of oblateness because a spherical planet can only pro-

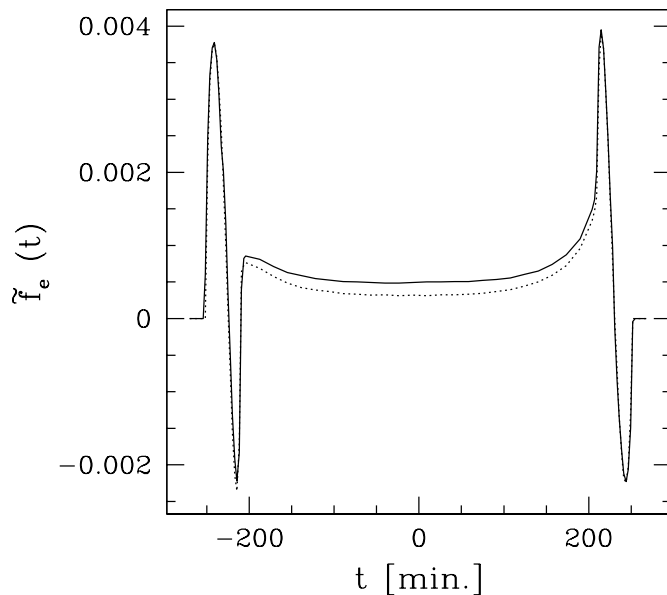


FIG. 10.—Fractional difference between the light deficit from an elliptical fiducial model and a spherical model, \tilde{f}_e (eq. [17]), with parameters of the spherical model tuned to minimize this fractional difference. The solid line is for a model with lensing, and the dotted line is for a model without lensing. The derived parameters of the spherical planet are $R_0 = 35,230$ km, $u_* = 0.8048$, and $v_* = -0.227$ for the lensed case (solid line) and $R_0 = 35,270$ km and the same u_* and v_* for the unlensed case (dotted line). The dotted line is essentially the fractional difference in the light deficit of an elliptical compared to a spherical planet of a similar total area. See text for details.

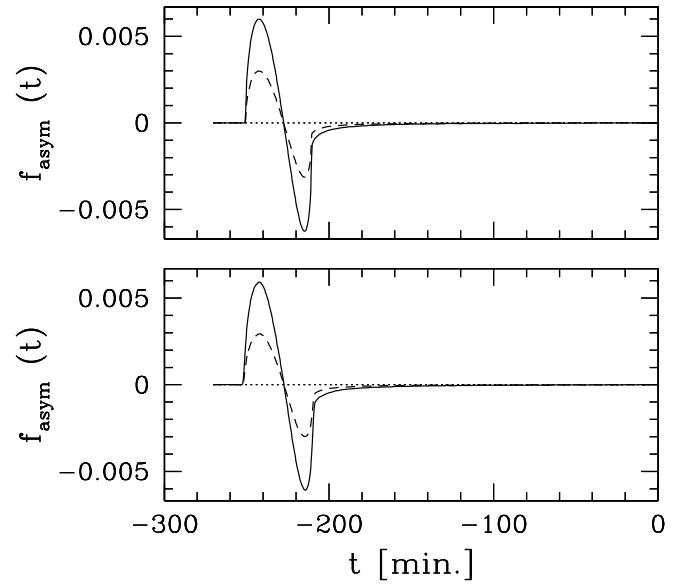


FIG. 11.—Value of f_{asym} as defined in eq. (18) with (bottom) and without (top) lensing. The solid line is for $\epsilon = 0.1$, the dashed line is for $\epsilon = 0.05$, and both are for $\gamma_{\text{tr imp}} = 45^\circ$. The dotted line is for the same ϵ but with $\gamma_{\text{tr imp}} = 0^\circ$. In all cases, the rest of the parameters are those of the fiducial model (filled square in Fig. 3). If the curves in the upper and lower panels are plotted together, they almost completely overlap; i.e., light curves with and without lensing have an almost identical degree of oblateness-induced asymmetry.

duce symmetric light curves. We show in Figure 11 the following fractional difference:

$$f_{\text{asym}}(t) = \frac{\Delta F(t) - \Delta F(-t)}{\Delta F^{\max}}. \quad (18)$$

The solid line denotes the case for $\epsilon = 0.1$ and the dashed line for $\epsilon = 0.05$, both for $\gamma_{\text{tr imp}} = 45^\circ$. The dotted line shows the same for $\gamma_{\text{tr imp}} = 0^\circ$, verifying that the asymmetry vanishes for exact alignment of the major (or minor) axis with the direction of motion. The lower panel shows $f_{\text{asym}}(t)$ where all quantities are evaluated with lensing, while the upper panel shows the same without lensing. The sets of curves are almost identical. This means the degree of asymmetry in the light curve is determined by the size of the oblateness and angle $\gamma_{\text{tr imp}}$ alone and is insensitive to lensing.

6. ABSORPTION AND COLOR DEPENDENCE

6.1. More Accurate Modeling of Absorption and Its Effects on Lensing

So far we have been using a crude step function model of absorption that turns abruptly on and off at $u = R_0/D_{OL}$. Here we use absorption to refer to extinction by either absorption or scattering. Taking into account absorption in a more realistic way is, in principle, straightforward. For each image position, there is an associated optical depth:

$$\begin{aligned} \tau(\theta_I) &= \int_{-\infty}^{\infty} \sigma \frac{\rho}{\mu m_H} dz \\ &= \frac{\rho_0}{\mu m_H} \sigma \sqrt{2\pi u D_{OL} H} \exp\left(-\frac{u D_{OL} - R_0}{H}\right), \end{aligned} \quad (19)$$

where u is defined in terms of θ_I as in equation (6), and we

have used the condition that $uD_{OL}/H \gg 1$. The symbol μm_H denotes the mean molecular weight. To compute the light curve with absorption, $W(\theta_I)$ should be replaced by $e^{-\tau(\theta_I)}$ in equation (7).

The absorption cross section σ can vary significantly depending on the composition of the planet atmosphere and the wavelength of interest and is essentially infinite at the surface of a rocky planet. To demonstrate concretely the effect of more accurate, gradual absorption, we adopt the cross section appropriate for Rayleigh scattering (Jackson 1999):

$$\sigma = 10^{-27} \text{ cm}^2 \left(\frac{5000 \text{ \AA}}{\lambda} \right)^4, \quad (20)$$

where λ is the wavelength of interest.

We recompute predictions for the fiducial model (filled square in Fig. 3) using the model outlined above. In Figure 12, we show the following fractional difference,

$$f_a(t) = \frac{\Delta F_{ab}(t) - \Delta F(t)}{\Delta F_{ab}^{\max}}, \quad (21)$$

where $\Delta F_{ab}(t)$ represents the deficit computed when a gradual change in absorption is used, while $\Delta F(t)$ denotes the same computed with a step function approximation for W (eq. [8]). The upper solid and dotted lines in Figure 12 give the above quantity with or without lensing. Gradual absorption produces light curves that are different from a step function absorption/occultation at about the 1% level. The above uses the same planet radius R_0 for ΔF_{ab} and ΔF . This difference can be much diminished, however, if one chooses an appropriate R_0 for the step function model. The lower solid and dotted lines in Figure 12 are the minimized

fractional difference,

$$\tilde{f}_a(t) = \frac{\Delta F_{ab}(t, R_0) - \Delta F(t, R'_0)}{\Delta F_{ab}^{\max}(R_0)}, \quad (22)$$

for cases with and without lensing, respectively, where we tune R'_0 to make \tilde{f}_a small. The small value of $\tilde{f}_a(t)$ in Figure 12 shows that our step function absorption model is actually a good approximation to reality—a suitable R_0 can always be found such that it approximates a gradual absorption model to high accuracy. This works primarily because $e^{-\tau}$ does behave almost like a step function because of the fact that ρ and therefore τ vary exponentially with radius.

With the above results we can proceed to discuss the color dependence of a transit light curve. There are three main factors. First, the stellar profile changes with wavelength, generally flatter as one considers redder wave bands (see § 3). Second, the refractive coefficient α varies with wavelength. The variation depends on atmosphere composition, and some examples are given in Table 1. Third, the absorption cross section σ also varies with wavelength. In fact, for Rayleigh scattering, for instance (eq. [20]), absorption varies much more strongly with wavelength compared to both the index of refraction and limb darkening. This can have a dramatic consequence for the existence of caustics. Consider a model like the open square in the B - R_0/H plane as shown in Figure 3. Recall that $B = (2\alpha\rho_0/H)[D_{OL}D_{LS}/(D_{OL} + D_{LS})]$ (eq. [9]). As one considers shorter wavelengths or bluer colors, σ becomes larger, increasing the optical depth (eq. [19]). In our step function model, this is equivalent to lowering ρ_0 (defined to be the density at which $\tau = 1$), in other words, lowering B .¹⁰ For sufficiently blue colors, the model would shift down from the open square in Figure 3 and cross the strong lensing threshold (*solid line*), erasing the caustics and making the lensing signal much weaker (as discussed in § 5.2). The same also holds true at wave bands where other kinds of absorption are important, such as molecular electronic absorption bands in the UV and rotational-vibrational bands in the IR of species such as H_2O , CO_2 , and CH_4 . This is a well-known result for solar system planet occultations of distant stars where lensing effects are strong in the optical but nonexistent in the UV and within strong absorption bands in the IR.

In summary, for extrasolar planet transits where caustics exist, we expect the lensing signal to disappear or at least weaken at wave bands with high extinction.

6.2. Planetary Atmosphere Transmission Spectrum and Stellar Spectrum

Extrasolar planet transit transmission spectra have been described in several papers for both the close-in extrasolar giant planets (Seager & Sasselov 2000; Brown 2001; Hubbard et al. 2001) and Earth-like planets (Schneider 1994; Webb & Wormleaton 2001). For parameters with strong lensing (Fig. 2), the transmission spectrum could be significantly affected by atmospheric refraction. At wave bands corresponding to the transparent continuum, strong lensing

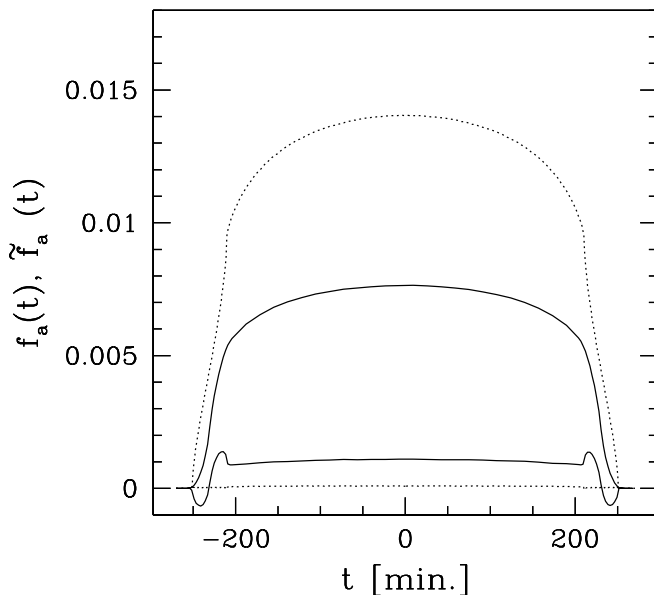


FIG. 12.—The $f_a(t)$ (eq. [21]) for cases with and without lensing (*upper solid and dotted lines, respectively*). The lower solid and dotted lines show the corresponding $\tilde{f}_a(t)$ (eq. [22]), which is a minimized function. The small values of the lower two lines demonstrates that an appropriate R_0 can always be chosen so that the step function model approximates a more realistic absorption model to high accuracy.

¹⁰ Changing σ also changes our definition of R_0 , which is where $\tau \sim 1$. While this does affect the transit light curve somewhat, its effect on lensing is smaller compared with that due to ρ_0 . This is because varying σ typically changes R_0 by a few scale heights H , and that represents a small change to R_0/H (since $R_0 \gg H$), which is the other parameter that controls the lensing behavior.

can lower the flux (recall from § 5.1 that lensing generally causes a net suppression of flux during most of the transit), while as we have discussed in the last subsection, at wave bands corresponding to strong planetary absorption bands, lensing has negligible effects. The contrast between continuum and absorption lines is therefore decreased, and effective line strengths are therefore altered.

The magnitude of this effect can be estimated as follows: The atmospheric lensing effect generally introduces a decrease in absolute flux that is approximately $(R_0/R_*)^2(H/R_0)$ for planets with caustics. Strong planetary atmosphere absorption lines, on the other hand, cause a change in absolute flux that is approximately $(R_0/R_*)^2x(H/R_0)$, where $x \sim$ a few. Therefore, in a planetary transmission spectrum, the effective line strength is reduced from $x(H/R_0)$ to $\sim(x-1)(H/R_0)$. The exact size of this effect depends on details of the atmospheric structure and composition as well as the limb-darkening function.

As noted in our Figure 3 and commented on previously (Seager & Sasselov 2000; Hubbard et al. 2001; Brown 2001), the transmission spectra of the close-in extrasolar giant planets (EGPs)—including the only known transiting EGP, HD 209458b—will be little affected by refraction because caustics do not exist because of the small planet-star distance (see § 5.1).

Finally, we end this section by briefly commenting on the stellar spectrum. During a planetary transit, the stellar spectrum changes with time, a phenomenon referred to as a spectroscopic transit. There are at least two different effects. The first has been discussed and observed by Queloz et al. (2000). The planet blocks different parts of the rotating stellar disk as the transit progresses, causing redshifting or blue-shifting of the stellar lines during the transit. The second effect arises from the fact that different parts of spectral lines and different lines are formed at different depths in the stellar atmosphere. As the planet transits different parts of the limb-darkened stellar disk, the stellar line shapes and strengths changes. Atmospheric lensing introduces modifications to both of the above effects because flux from different parts of the star is magnified compared to the nonlensed case.

7. DISCUSSION

Our findings are summarized as follows:

1. The importance of atmospheric lensing is mainly controlled by two parameters: R_0/H (the ratio of planet radius to atmospheric scale height) and $B \equiv 2\alpha\rho_0D_{LS}/H$ (product of the refractive coefficient, atmospheric density, and star-planet separation divided by the scale height).¹¹ The condition for strong lensing—the existence of caustics—is described by equation (13) and depicted in Figure 3. When applying our results, it is important to keep in mind that ρ_0 is the atmospheric density at an impact parameter such that the optical depth is unity (see § 6.1).

2. Strong lensing generally introduces a fractional change in the light deficit on the order of H/R_0 during a planetary transit. We choose to discuss changes induced by lensing in terms of fractional changes in the light deficit $[f(t)]$ as defined in eq. (14) and shown in, e.g., Fig. 6] so that the

absolute change in observed flux can be easily estimated for any planet-to-star size ratio.¹² It works as follows: The drop in flux during a nonlensed transit is about $(R_0/R_*)^2$, where R_* is the radius of the star. Strong lensing introduces an additional absolute change in flux that is therefore about $(R_0/R_*)^2(H/R_0)$.

3. Lensing produces a characteristic slowing down in the dimming of the starlight at ingress (reversed at egress). This is due to the additional photons refracted into view from the planet's shadow. The light curve of a lensed transit can be mimicked to some extent by one of a nonlensed transit if parameters for the latter are appropriately tuned. We find, however, that the difference between the two can remain significant especially during ingress and egress. For example, the dotted line in Figure 6 shows a fractional difference in the light deficit of $\sim 0.5(H/R_0)$ at ingress or egress. When this difference is larger than the observational uncertainties, we should be able to constrain the lensing signal parameters such as the atmospheric scale height, density, and refractive coefficient (parameters such as R_0 and D_{LS} can be learned from other features of the light curve or other observations). The scale height and refractive coefficient will in turn give us useful information on the temperature and chemical composition of the planet.

4. The strength of lensing is expected to vary significantly with color. The primary reason is the variation of absorption and scattering with wavelength. In wave bands where absorption or scattering is significant, caustics are effectively hidden by extinction. Therefore, the optimal wave bands for detecting atmospheric lensing is toward the red or near infrared, where the inevitable Rayleigh scattering is less strong, but away from strong absorption bands such as gaseous H_2O or CH_4 . Optically thick clouds (such as enstatite in hotter planets or H_2O or CH_4 ice in cooler planets) might contribute significant opacity. See Hubbard et al. (2001) for a detailed treatment of HD 209458b.

5. Several conditions are therefore advantageous for detecting the lensing signal: (a) observations at wave bands where absorption and scattering is weak, (b) a high temperature of the planet atmosphere due to a nearby hot star, which raises the atmospheric scale height (thereby increasing H/R_0), and (c) D_{LS} large enough to keep $B \equiv 2\alpha\rho_0D_{LS}/H$ above the strong lensing threshold. Our fiducial model (filled square in Fig. 3) provides an example in which lensing induces a fractional change in the light deficit of around 1%. For a planet that has an area about 1% of the star, this implies that lensing causes an absolute change of about 10^{-4} in the normalized flux—an observationally relevant effect. This model can be realized by a gaseous giant (similar to Jupiter in mass but with a slightly inflated radius due to high temperature) about an AU away from an A star, with observations done in red wave bands ($\lambda \sim 10^4 \text{ \AA}$) but away from possible strong absorption bands such as water. We should emphasize there is considerable uncertainty in the size of such a planet because the radius of a hot gaseous giant varies significantly with time (Burrows et al. 2000; see also Murray et al. 1998 and Lin et al. 2000 on change in orbital characteristics over time).

6. Oblateness of the planet induces an asymmetry to the transit light curve (about the point of minimum flux), which

¹¹ In the solar system case, D_{LS} is replaced by D_{OL} ; see § 4.3.

¹² The observed stellar flux here is always normalized by its pre- or post-transit value.

vanishes only when the semimajor or semiminor axis of the planet is exactly aligned with the direction of relative motion. The asymmetry is about 0.5%, as measured in fractional light deficit (eq. [18] and Fig. 11), for a projected oblateness or ellipticity of $\epsilon = 0.1$ and an angle of 45° between the semimajor axis and direction of motion. The absolute difference in flux between ingress and egress is therefore about $0.5\% \times (R_0/R_*)^2$ and is, for example, 5×10^{-5} for a planet that is 1/10 the size of the star.

7. For HD 209458b, the only currently known transiting extrasolar planet, caustics and therefore strong lensing are absent because of the very small lens-source separation (and the resulting large scale height due to a high temperature). Its oblateness is expected to be small, $\lesssim 10^{-3}$, because of the tidal locking of its rotation to orbital motion.

In this paper we have focused on the effects of atmospheric lensing and planet oblateness on the transit light curve. It is worthwhile to briefly list other possible “secondary” fluctuations to the light curve—variations in the observed flux other than those due to the standard spherical occultation of a star with a smooth limb-darkening profile. They can be divided into three categories.

The first category is due to close companions of the planet. Rings and moons, if present, induce an asymmetry to the light curve that may be confused with oblateness. They also introduce additional parameters that control the light curve, making it perhaps more difficult to discern the lensing signal. Taking Jupiter as an example, the largest moon Ganymede has a radius of 2635 km, about 3.7% the size of Jupiter. The same moon of a Jupiter-like planet orbiting another star would induce a fractional change of about 10^{-3} in the light deficit. This is about 5–10 times smaller than the lensing or oblateness effects we found for our most optimistic models (Figs. 6 and 11). If the moon is sufficiently far from the planet, it might also introduce distinct signatures at ingress or egress (see, e.g., Sartoretti & Schneider 1999) that can be disentangled from oblateness or lensing effects. An opaque ring half the size of Saturn’s rings for a gaseous giant with $R_p = 1.4R_J$ orbiting a Sun-like star would deepen the planet transit light curve by 0.05%–1.2% depending on the inclination of the ring (Seager & Hui 2002b). Ring effects might be isolated by looking for distinct shapes in the transit light curve (see Brown et al. 2001) and possibly rescattered starlight.

The second category is due to the planet itself. The planet atmosphere can have persistent or transient disturbances that modify the transit light curve. Such disturbances have to be large in extent to change the light curve significantly. For instance, small uniformly distributed clouds would not introduce an asymmetry to the light curve. Something like the Great Red Spot on Jupiter could conceivably be large enough, but such disturbances cannot introduce a fractional change in the light deficit that is larger than the ratio of the projected atmospheric area to total planetary area, i.e., $\sim H/R_0$. It is important to emphasize that perturbations to the atmosphere that only change the effective radius of the planet R_0 are not sufficient to wash out the lensing signal; as we have shown in § 5.2, just tuning R_0 is not enough to confuse a lensed transit with a nonlensed transit that has different parameters. Hubbard et al. (2001) pointed out that Rayleigh scattering, in addition to causing extinction, also produces a glow around the planet, which changes its effective size (fractional variation in size of about 1% between

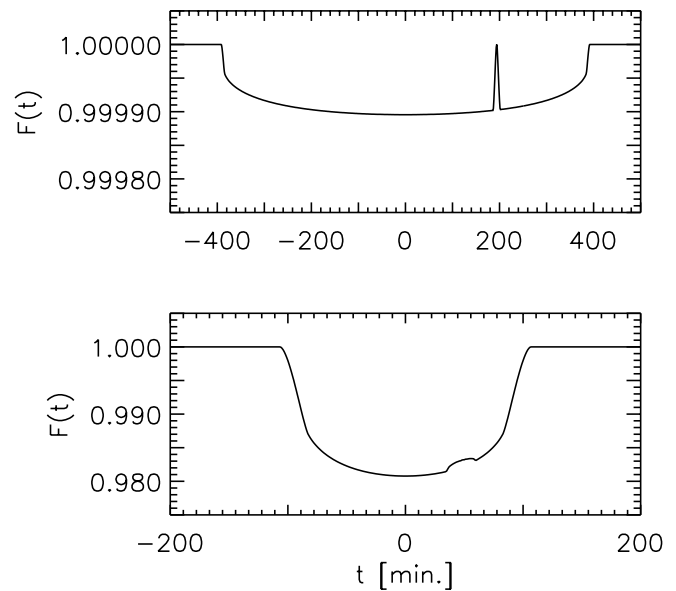


FIG. 13.—Effect of a planet crossing an Earth-sized star spot on a stellar disk. *Top*: An Earth-like planet transit. *Bottom*: A close-in EGP-like planet transit.

different wavelengths). It would be interesting to explore how both Rayleigh and condensate rescattered stellar photons affect the detailed shape of the transit light curve (i.e., aside from a simple change in R_0). Finally, we have also ignored diffraction in this paper. Diffraction is likely unimportant for most extrasolar cases of interest for two reasons. First, the relevant parameter combination $(R/H)^{1/2} BD_{OL}/D_{LS}$ is greater than unity (see Fig. 3) and is therefore not favorable for diffraction (see, e.g., French & Gierasch 1976; Elliot et al. 1975). Second, the observed flux comes from a sum over incoherent sources distributed over the stellar surface.

The third category of secondary fluctuations is due to complications in the star. Stellar oscillations are expected to produce absolute changes in the flux at a 10^{-5} level on the timescale of a transit.¹³ Also, realistic stellar profiles might have bumps and wiggles on top of the smooth profile we have assumed (eq. [10]). For instance, the light curve would be modified if a planet happens to transit over a star spot (see, e.g., Seager & Hui 2002b). The largest effect is obtained if the spot has a size that is comparable to the planet and the planet happens to overlap completely with the spot during the transit. At the point where the planet and spot coincide, the flux would basically return to unity, its pretransit value. For example, an Earth-sized planet that happens to cross over an Earth-sized star spot would produce this behavior, as illustrated in the upper panel of Figure 13. This kind of situation is probably rare, however, particularly if the planet considered is a gaseous giant, i.e., much larger than typical star spot (lower panel of Fig. 13). Then the absolute change in flux in such coincident transits will be roughly the ratio of the spot area to star area, $\lesssim 10^{-5}$, borrowing from the example of the Sun. Note also that while lensing or oblateness effects are most easily recognized at ingress or

¹³ See, e.g., the Web site for the proposed Kepler mission at <http://www.kepler.arc.nasa.gov>.

egress, changes to the light curve due to imperfections in the stellar profile can occur throughout the transit. More detailed studies would be required to see if spots produce different signatures from lensing or oblateness if the planet crosses them at ingress or egress. Note also that effects due to star spots are likely not repeatable over many planetary periods.

It is also worth emphasizing that even in cases in which the lensing or oblateness signal is weak and therefore not easily isolated, it could still act as an important contaminant in confusing other signals one might be interested in, such as detection of moons and planetary rings. From the above discussions, it is clear that future high-precision measurements of extrasolar planetary transits will present a very interesting challenge—there are several sources of small secondary fluctuations (change in flux of 10^{-4} or less) that are

within observational reach and that would require some effort to disentangle. The rewards of such efforts will be substantial—from detection of moons and rings to measuring the (projected) planet oblateness, and therefore constraining its rotational period, and from studies of the stellar atmosphere to studies of the planetary atmosphere, constraining, for instance, its scale height, temperature, density, and composition.

We are grateful to John Bahcall, Bruce Draine, Scott Gaudi, Joe Patterson, and Penny Sackett for useful discussions. We thank our referee, William Hubbard, for a careful reading of the manuscript and helpful suggestions. S. S. is supported by the W. M. Keck foundation, and L. H. is supported by the Taplin Fellowship at the IAS and an Outstanding Junior Investigator Award from the DOE.

APPENDIX A

Here, we would like to motivate the density profile we adopt in this paper. We begin by the following statement of hydrostatic equilibrium of the atmosphere:

$$\nabla P = -\rho \nabla \phi_{\text{eff}}, \quad (\text{A1})$$

where P is the pressure and ϕ_{eff} is an effective potential that is the sum of the gravitational potential ϕ and a potential to take into account rotation:

$$\phi_{\text{eff}} = \phi - \frac{1}{2} \omega^2 (x'^2 + y'^2), \quad (\text{A2})$$

where z' is the axis of rotation, x' and y' are the perpendicular axes (we will use x'_i , $i = 3, 1, 2$ to denote them), and ω is the angular speed. For an isothermal atmosphere where $P \propto \rho$, the above implies

$$\rho \propto \exp(-\phi_{\text{eff}}). \quad (\text{A3})$$

We note that planetary atmospheres are only approximately isothermal. Deviations such as temperature inversion are known to exist (see, e.g., Jones 1999).

The question then reduces to what kind of gravitational potential one expects for a general rotating figure of equilibrium. For bodies that are not too aspherical, we can expand the gravitational potential using the Legendre polynomials (see, e.g., Danby 1962; Chandrasekhar 1969)

$$\phi = -\frac{GM_p}{r'} \left[1 - \frac{J_2}{r'^2} \frac{1}{2} (3 \cos^2 \theta - 1) - \dots \right], \quad (\text{A4})$$

where M_p is the planet mass, J_2 is some constant coefficient that is presumably small, θ is the angle between the radial vector and the z' -axis, and $r' = (x'^2 + y'^2 + z'^2)^{1/2}$. It is sufficient to illustrate our argument using only the first term—it is possible to generalize to include higher order terms in the potential expansion.

We are interested in the form of ϕ_{eff} when $r' = R(1 + \eta)$ with $\eta \ll 1$, where R is approximately the planet radius. We are also interested in cases in which the angular speed ω is in some sense small—the relevant parameter to consider is $R^3 \omega^2 / (2GM_p) \equiv \delta \ll 1$. One can then express ϕ_{eff} as

$$\begin{aligned} \phi_{\text{eff}} &= -\frac{GM_p}{r'} - \frac{1}{2} \omega^2 (x'^2 + y'^2) \\ &\sim -2 \frac{GM_p}{R} + \frac{GM_p}{R^2} \sqrt{x'^2 + y'^2 + z'^2} - \frac{1}{2} \omega^2 (x'^2 + y'^2) \\ &\sim -2 \frac{GM_p}{R} + \frac{GM_p}{R^2} \left[\frac{x'^2}{(1 + \delta)^2} + \frac{y'^2}{(1 + \delta)^2} + z'^2 \right]^{1/2}, \end{aligned} \quad (\text{A5})$$

which is exact up to terms of first order in η and δ . Clearly, ϕ_{eff} is a function of r alone, where $r^2 \equiv \sum_i x_i'^2 / a_i^2$, where $a_1 = a_2 = 1 + \delta$ and $a_3 = 1$. In the above derivation $a_1 = a_2 \neq a_3$. A rotating body of self-gravitating fluid can actually be triaxial in general, but triaxiality is likely unimportant for the rotational velocities of interest here (see Chandrasekhar 1969; Bertotti & Fasina 1990).

Putting the above into equation (A3), we obtain

$$\rho = \rho_0 \exp\left[\frac{-(r - R_0)}{H}\right], \tag{A6}$$

where H^{-1} is the derivative of the effective potential and ρ_0 is the atmospheric density at $r = R_0$. The choice of R_0 is arbitrary at this point. In § 2.1, we choose it to be the radius below which the atmosphere is completely opaque.

Finally, note that the principle axes defined by x'_i are not necessarily lined up with the axes defined by x_i in § 2.1 by the lensing geometry. The two sets are generally related by a rotation. Since there is freedom in rotating x_1 and x_2 (i.e., the lensing geometry only picks out x_3 or the z -direction), we can without loss of generality relate the two sets of coordinates by two rotation matrices: $\mathbf{x}' = \mathbf{R}_{z'}(\gamma) \cdot \mathbf{R}_{x'}(\beta) \cdot \mathbf{x}$, where $\mathbf{R}_{z'}(\gamma)$ is a rotation about x'_3 by angle γ and $\mathbf{R}_{x'}(\beta)$ is a rotation about x'_1 by angle β . Using $a_1 = a_3(1 + \epsilon_A)$ and $a_2 = a_3(1 + \epsilon_B)$ and assuming that ϵ_A and ϵ_B are small (in our above derivation, $\epsilon_A = \epsilon_B = \delta$, i.e., an oblate spheroid; our derivation below continues to work even if this were violated), we can write

$$r^2 = \tilde{z}^2 + (1 - 2\epsilon_A \cos^2 \gamma - 2\epsilon_B \sin^2 \gamma)x^2 + 4(\epsilon_A - \epsilon_B)xy + (1 - 2\epsilon_A \sin^2 \gamma \cos^2 \beta - 2\epsilon_B \cos^2 \gamma \cos^2 \beta)y^2, \tag{A7}$$

where $\tilde{z} = [1 + O(\epsilon_A, \epsilon_B)][z + O(\epsilon_A, \epsilon_B)x + O(\epsilon_A, \epsilon_B)y]$.

Now, recall that the quantity that we are interested in, the deflection angle θ_D , is given by equation (2): $\theta_D = \nabla_{\perp} \int_{-\infty}^{\infty} \alpha \rho(r) dz$. One can clearly change the variable of integration from z to \tilde{z} : $\int_{-\infty}^{\infty} \alpha \rho_0 \exp[-(r - R_0)/H] dz = \int_{-\infty}^{\infty} \alpha \rho_0 \exp[-(r - R_0)/H] d\tilde{z}$, where we have absorbed the slight change in multiplicative factor into a redefinition of ρ_0 . Moreover, since \tilde{z} is a dummy integration variable, we could as well rename $\tilde{z} \rightarrow z$ in equation (A7).

Consider next the terms involving x and y in equation (A7). We could easily perform a rotation to put them in the simple form: $(1 - \epsilon)x^2 + (1 + \epsilon)y^2$ if we absorb multiplicative factors into a redefinition of H (such multiplicative factors would affect z also, but they can once again be absorbed into redefinition of ρ_0). To be more specific, let us consider the important case in which $\epsilon_A = \epsilon_B$. Then, the x and y terms reduce to

$$(1 - 2\epsilon_A)x^2 + (1 - 2\epsilon_A \cos^2 \beta)y^2 = [1 - \epsilon_A(1 + \cos^2 \beta)][(1 - \epsilon)x^2 + (1 + \epsilon)y^2], \tag{A8}$$

where

$$\epsilon = \epsilon_A(1 - \cos^2 \beta). \tag{A9}$$

For a random distribution of angle β , we expect on the average $\epsilon = \epsilon_A/2$. It is unclear, however, if β should be randomly distributed. The solar system planets do seem to have rotational axes pointing in all kinds of directions with respect to their orbital planes. The quantity ϵ_A describes directly the shape of the planet: contours of constant density obey $z^2 + (x^2 + y^2)/(1 + \epsilon_A)^2 = \text{constant}$. In other words, oblateness, defined by the ratio $(a_1 - a_3)/(a_1 + a_3)$, is given by $\epsilon_A/2$ to the lowest order. One can view ϵ as a kind of projected ellipticity or oblateness.

To summarize, with suitable rescaling of z , H , and ρ_0 , we have

$$\theta_D = \int_{-\infty}^{\infty} \alpha \rho_0 \exp\left[\frac{-(r - R_0)}{H}\right] dz, \quad r^2 = (1 - \epsilon)b_1^2 + (1 + \epsilon)b_2^2 + z^2, \tag{A10}$$

where we have equated x and y with impact parameters b_1 and b_2 as defined in § 2.1.

APPENDIX B

We discuss here how to solve equation (5) and how to find the caustic and critical curve. Equation (5) has a form that is exactly analogous to elliptic potentials sometimes used in modeling gravitational lenses. The main trick for solving this type of lensing equation is taken directly from Schneider, Ehlers, & Falco (1992), but we provide additional comments here for cases that require special attention.

Equation (5) is a set of two equations for θ_I^1 and θ_I^2 , given the source position θ_S . Eliminating $\psi(u)$ from the two equations, one obtains

$$\theta_I^2 = \frac{(1 - \epsilon)\theta_I^1 \theta_S^2}{(1 + \epsilon)\theta_S^1 - 2\epsilon\theta_I^1}. \tag{B1}$$

This gives us θ_I^2 as a function of θ_I^1 , and substituting into the first component of the lensing equation leaves us with a single equation for θ_I^1 :

$$\theta_S^1 = \theta_I^1 + (1 - \epsilon)\theta_I^1 \psi(u), \tag{B2}$$

where u is a function of θ_I^1 and θ_I^2 (now a function of θ_I^1) as well. The lensing problem is therefore no more complicated than one with spherical symmetry. Once θ_I^1 is solved for, θ_I^2 can be obtained from equation (B1).

For the case of $\theta_S^2 = 0$, the above solution always puts $\theta_I^2 = 0$. There is, however, another possibility when multiple images are allowed. Examining the analog of equation (B2) for the second component, one can see that the other option for a vanish-

ing θ_S^2 is to have

$$1 + (1 + \epsilon)\psi(u) = 0. \quad (\text{B3})$$

This gives a single equation for θ_I^2 if one uses the fact that $\theta_I^1 = (1 + \epsilon)\theta_S^1(2\epsilon)^{-1}$. This is obtained from eliminating $\psi(u)$ from the two components of equation (5) but noting $\theta_S^2 = 0$ and assuming $\theta_I^2 \neq 0$.

There is another special case: $\theta_S^1 = 0$. In this case, equation (B2) tells us that there are two possibilities: $1 + (1 - \epsilon)\psi(u) = 0$ or $\theta_I^1 = 0$. The former is handled automatically with the computational procedure above. The latter requires more care: one can solve

$$\theta_S^2 = \theta_I^2 + (1 + \epsilon)\theta_I^2\psi(u) \quad (\text{B4})$$

for θ_I^2 by setting $\theta_I^1 = 0$. Doing so ensures that all possible images are uncovered.

To find the caustic and critical curve, we solve $A^{-1} = 0$ using equation (6):

$$v = \frac{-1}{\epsilon\tilde{\psi}} [1 + 2\psi + (1 - \epsilon^2)\psi^2 + (1 - \epsilon^2)u^2\psi\tilde{\psi} + u^2\tilde{\psi}]. \quad (\text{B5})$$

This gives us v for a given u . However, from the definition of v and u in equation (6), it is clear that only $|v| \leq u^2$ is physical. Therefore, the caustic or critical curve corresponds to solutions of v given u that satisfies $|v| \leq u^2$. Strong lensing occurs when such solutions exist. For each pair of v and u , it is easy to solve for θ_I^j from their definitions:

$$\theta_I^1 = \pm \sqrt{\frac{u^2 - v}{2(1 - \epsilon)}}, \quad \theta_I^2 = \pm \sqrt{\frac{u^2 + v}{2(1 + \epsilon)}}. \quad (\text{B6})$$

Given the critical curve defined by θ_I^j , one can then solve for the caustic using the lens mapping (eq. [5]). We note that the above two expressions were interchanged by mistake in Schneider et al. (1992).

REFERENCES

- Bertotti, B., & Farinella, P. 1990, *Physics of the Earth and the Solar System* (Dordrecht: Kluwer)
- Born, M., & Wolf, E. 1999, *Principles of Optics: Electromagnetic Theory of Propagation, Interference and Diffraction of Light* (Cambridge: Cambridge Univ. Press)
- Brown, T. M. 2001, *ApJ*, 553, 1006
- Brown, T. M., Charbonneau, D., Gilliland, R. L., Noyes, R. W., & Burrows, A. 2001, *ApJ*, 552, 699
- Burrows, A., Guillot, T., Hubbard, W. B., Marley, M. S., Saumon, D., Lunine, J. I., & Sudarsky, D. 2000, *ApJ*, 534, L97
- Chandrasekhar, S. 1969, *Ellipsoidal Figures of Equilibrium* (New Haven: Yale Univ. Press)
- Charbonneau, D., Brown, T. M., Latham, D. W., & Mayor, M. 2000, *ApJ*, 529, L45
- Cox, A. N. 2000, *Allen's Astrophysical Quantities* (New York: AIP)
- Danby, J. M. A. 1962, *Fundamentals of Celestial Mechanics* (New York: Macmillan)
- Draine, B. T. 1998, *ApJ*, 509, L41
- Elliot, J. L., & Olkin, C. B. 1996, *Annu. Rev. Earth Planet. Sci.*, 24, 89
- Elliot, J. L., Wasserman, L. H., Ververka, J., Sargan, C., & Liller, W. 1975, *AJ*, 80, 323
- French, R. G., & Gierasch, P. J. 1976, *AJ*, 81, 445
- Henry, G. W., Marcy, G. W., Butler, R. P., & Vogt, S. S. 2000, *ApJ*, 529, L41
- Hubbard, W. B. 1997, *Science*, 278, 403
- Hubbard, W. B., Fortney, J. J., Lunine, J. I., Burrows, A., Sudarsky, D., & Pinto, P. A. 2001, *ApJ*, 560, 413
- Jackson, J. D. 1999, *Classical Electrodynamics* (New York: Wiley)
- Jha, S., Charbonneau, D., Garnavich, P. M., Sullivan, D. J., Sullivan, T., Brown, T. M., & Tonry, J. L. 2000, *ApJ*, 540, L45
- Jones, B. W. 1999, *Discovering the Solar System* (New York: Wiley)
- Lin, D. N. C., Papaloizou, J. C. B., Terquem, C., Bryden, G., & Ida, S. 2000, in *Protostars and Planets IV*, ed. A. Boss, V. Mannings, & S. Russell (Tucson: Univ. Arizona Press), 1111
- Mazeh, T., et al. 2000, *ApJ*, 532, L55
- Murray, N., Hansen, B., Holman, M., & Tremaine, S. 1998, *Science*, 279, 69
- Nicholson, P. D., McGhee, C. A., & French, R. G. 1995, *Icarus*, 113, 57
- Queloz, D., Eggenberger, A., Mayor, M., Perrier, C., Beuzit, J. L., Naef, D., Sivan, J. P., & Udry, S. 2000, *A&A*, 359, L13
- Sartoretti, P., & Schneider, J. 1999, *A&AS*, 134, 553
- Schneider, J. 1994, *Ap&SS*, 212, 321
- Schneider, P., Ehlers, J., & Falco, E. E. 1992, *Gravitational Lenses* (Berlin: Springer)
- Seager, S., & Hui, L. 2002a, *ApJ*, in press
- . 2002b, in *Planetary Systems in the Universe: Observations, Formation and Evolution*, ed. A. J. Penny, P. Artymowicz, A. M. Lagrange, & S. S. Russell, in press
- Seager, S., & Sasselov, D. D. 2000, *ApJ*, 537, 916
- Webb, J. K., & Wormleaton, I. 2001, *Publ. Astron. Soc. Australia*, 18, 252